The Astrophysical Journal, 701:298–305, 2009 August 10 doi:10.1088/0004-637X/701/1/298

STEREOSCOPIC RECONSTRUCTION FROM *STEREO*/EUV IMAGERS DATA OF THE THREE-DIMENSIONAL SHAPE AND EXPANSION OF AN ERUPTING PROMINENCE

A. Bemporad
INAF-Osservatorio Astronomico di Torino, Via Osservatorio 20, 10025 Pino Torinese (TO), Italy; bemporad@oato.inaf.it
Received 2008 December 16; accepted 2009 June 8; published 2009 July 22

ABSTRACT

On 2007 May 9, a prominence eruption was observed in the He II λ304 filter by the two EUV Imagers (EUVI) telescopes aboard the *STEREO A* and *B* spacecrafts. The high spatial resolution (∼1.″5 pixel^{-1}) EUVI images have been used to infer via triangulation the three-dimensional (3D) shape and orientation of the prominence ≃12 minutes after the beginning (13:40 UT) of the eruption. At this time, the prominence has the shape of a "hook" with the base anchored at the Sun. The "hook" prominence is highly inclined southward with respect to the radial direction, has an average thickness of 0.061 $R_\odot$, a length of 0.43 $R_\odot$, and lies in first approximation on a plane inclined by ∼54.°5 with respect to the line of sight. Thanks to the very high temporal cadence (∼37 s) of EUVI observations it has been possible also to infer the 3D early eruption trajectory. In the following ∼20 minutes the prominence rotates westward, undergoing a strong latitudinal acceleration, ∼3 times larger than the radial acceleration. In this time interval, the prominence expands in a direction mainly parallel to the plane of the sky; the total volume occupied by the plasma increases by a factor of ∼8, while the prominence thickness increases only by ∼12%. This is related to the fact that the early prominence expansion is anisotropic and occurs mainly on a plane parallel to the plane of the sky. Even if the small-scale spatial distribution of the erupting material observed in the He II EUVI images is quite complex, both the approximately planar shape and the successive planar expansion suggest that on larger spatial scales the prominence can be globally approximated as a two-dimensional "ribbon-like" feature, instead of a 3D twisted flux tube.

Key words: Sun: coronal mass ejections (CMEs) – Sun: prominences – Sun: UV radiation

Online-only material: color figures

1. INTRODUCTION

In the last few decades, a huge amount (∼10^4) of coronal mass ejections (CMEs) has been observed in remote sensing and in situ data and several techniques have been developed to infer their three-dimensional (3D) shapes and locations. Moran & Davila (2004) showed that it is possible to determine the 3D structure of a CME by using polarization measurements acquired by the *SOHO* Large Angle Spectrometric Coronagraph (LASCO; see Brueckner et al. 1995), while Cremades & Bothmer (2004) proposed an explanation for the observed differences in the projected aspects of CMEs depending on their 3D geometrical properties and on the neutral line orientation. Geometric 3D parameters of halo CMEs have been inferred from LASCO images by assuming a "cone model," i.e., a radial expansion able to preserve the CME angular width during the propagation through the corona (see, e.g., Zhao et al. 2002; Michalek et al. 2003; Xie et al. 2004) and several methods to infer the 3D location of CMEs have been proposed (see, e.g., Pizzo & Biesecker 2004; Inhester 2006). Great efforts have also been made in order to explain the observed CME morphologies as two-dimensional (2D) projections of an underlying 3D flux rope geometry with footpoints connected to the Sun (see, e.g., Chen et al. 1997; Dere et al. 1999; Wood et al. 1999).

However, the real 3D structure of these phenomena is still under debate. This is due both to the intrinsic large variety of the observed CME geometrical shapes and to the line-of-sight (LOS) projection effects of the optically thin coronal plasma which make observations from a single spacecraft (hence from a single point of view) ambiguous. Unique information on these topics have been derived in the last ∼12 years from the analysis of spectroscopic observations acquired by the *SOHO* Ultraviolet Coronagraph Spectrometer (UVCS; see Kohl et al. 1995). Spectroscopic observations of CMEs provided for the first time information both on the plasma velocity components along the LOS (thanks to the line Doppler shifts) and in the radial direction (thanks to the Doppler dimming/pumping effect; see Noci et al. 1987). The first CME observed by UVCS provided evidence for rotation of the velocity vector associated with helical motions of plasma around an erupted magnetic flux tube (Antonucci et al. 1997). The line intensity morphologies and line profile Doppler shifts have been used to infer the handedness of untwisting left-handed (Ciaravella et al. 2000) and right-handed (Suleiman et al. 2005) CME helixes and to verify that their handedness was in agreement with that of the pre-CME structures. The variations in the Doppler line shift observed in a CME in the H I Lyα line led Ciaravella et al. (2003) to conclude that the leading edge was not an hemispherical shell, but a loop- or ribbon-like structure. Nevertheless, the interpretation of spectroscopic CME data is often ambiguous because the effects of different physical phenomena (e.g., variations of plasma kinetic temperatures, densities, and bulk velocities integrated along the LOS) can be mixed.

The 3D ambiguities of CME observations can be resolved now by using data acquired from two different points of view by the pair of SECCHI EUV Imagers (EUVI; see Wuelser et al. 2004) aboard the twin *Solar Terrestrial Relations Observatory* (*STEREO*; see Kaiser et al. 2008) spacecrafts. Observations acquired from these instruments have already been used to infer the 3D shape of coronal loops (Feng et al. 2007) and polar plumes (Curdt et al. 2008). Recently, Mierla et al. (2008) estimated the propagation direction of CMEs by using the leading edges height–time curves measured from *STEREO COR-1 A* and *B* images, while

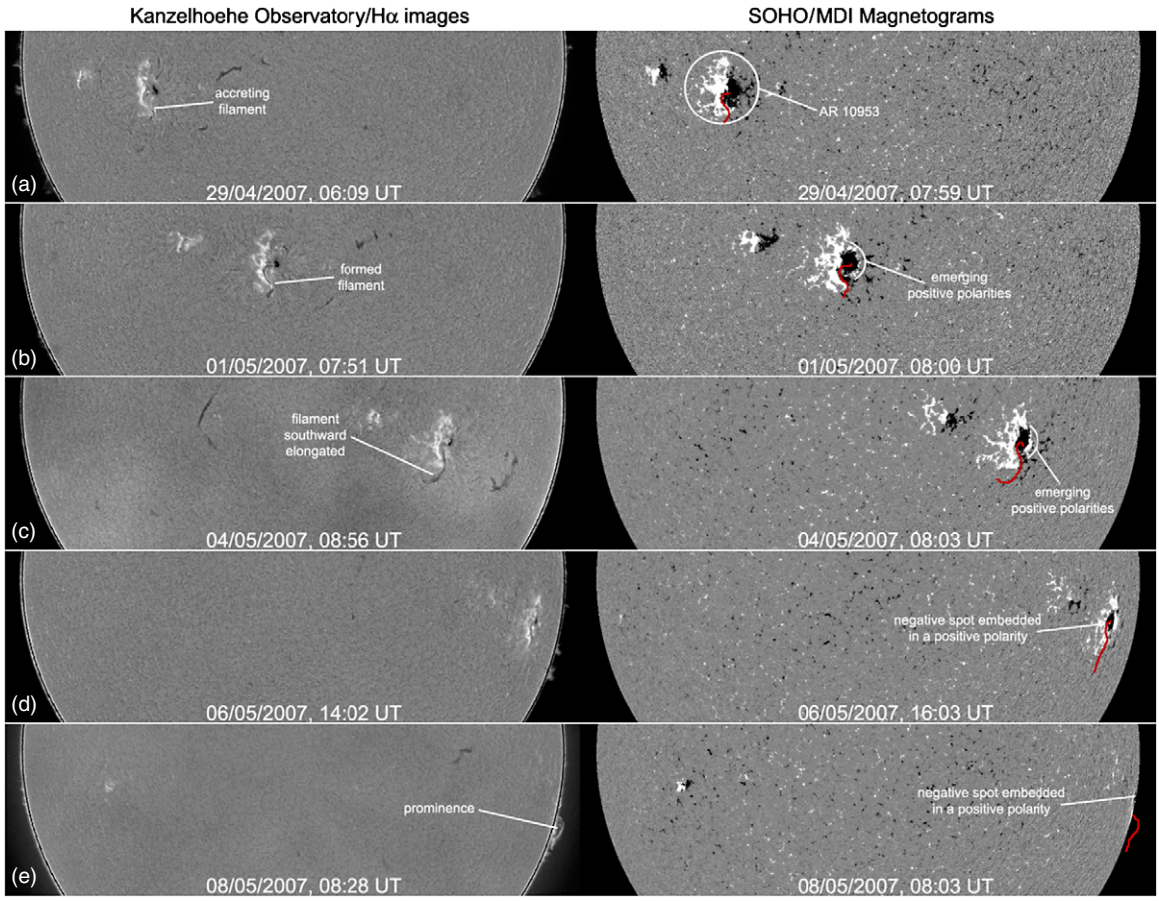

Figure 1. Left column: a series of Hα images acquired by the Kanzelhoehe Solar Observatory showing the evolution of the filament located above the AR 10953, source of the May 9 eruption. The filament, mainly aligned with the photospheric neutral line (see the right column) progressively lengthens southward (panels a–c) and at the time the AR crosses the solar limb is visible as a prominence located southward with respect to the AR latitude (panel e). Right column: a series of *SOHO*/MDI magnetograms showing the configuration of photospheric magnetic field during transit across the disk of AR 10953. This sequence shows the progressive emergence of a positive polarity (panels b–d) located westward of the negative polarity spot; the solid curved line represents the position of the filament, as derived from Hα images (left column).

(A color version of this figure is available in the online journal.)

Timothy & Tappin (2008) inferred by triangulation the position of the source region of two CMEs. Gissot et al. (2008) developed an algorithm to reconstruct from a pair of EUVI images a map of heights above the solar surface across an erupting filament and an erupting prominence has also been studied in three dimension by Thompson (2008a) who found a prominence rotation by $\sim$140° in the rising phase. However, only a few events have been studied so far in three dimension in their early erupting phase and the global picture of CME development is far from being completely understood. In this work, I report on the 3D reconstruction made from *STEREO* EUVI *A* and *B* data of the shape and trajectory of a prominence which erupted on 2007 May 9. After a general description of the event (Section 2), the technique used to infer the 3D prominence structure and trajectory from EUVI images is described in Section 3, while the results and the associated uncertainties are given in Section 4. Conclusions are summarized and discussed in Section 5.

2. THE 2007 MAY 9 FILAMENT ERUPTION

Between 2007 April 25 and May 8, the active region (AR) NOAA 10953, located at a latitude of $\sim$10° S, crosses the disk dragged by the solar rotation. An Hα "S-shaped" filament was visible in these days in this AR, mostly aligned along the north–south direction (Figure 1, left column): this filament is probably the source of the final prominence eruption observed on May 9. Hα images acquired by the Kanzelhoehe Solar Observatory in the days before the eruption show that the filament progressively grows and elongates southward (Figure 1, panels a–c). This evolution is probably linked to the AR activity as observed in the EUV: images acquired in the He II λ304 line by the two *STEREO A* and *B* EUVI telescopes show that this AR is highly unstable. Chromospheric material is continuously ejected southward in a sequence of small homologous eruptions unable to escape from the Sun, because the ejected material flows back along closed field lines, partially dragged by the solar gravitational force; a couple of these "failed" eruptions are shown in Figure 2 (top and bottom rows). The net result is a progressive accumulation of plasma southward of the AR source of the eruptions. It is likely that these small-scale "failed" eruptions, occurring at an approximate rate of $\sim$8–10 events per day, progressively fill the filament channel by chromospheric material, leading to a mass loading and finally to the observed growth and lengthening of the Hα filament.

In the "mass loading" CME model (see, e.g., Zhang & Chye Low 2005, for a recent review), solar eruptions are explained by the accumulation of mass suspended in unstable equilibrium by the magnetic field lines; the eruption is then initiated by a loss of anchoring mass or a variety of instabilities. Magnetograms

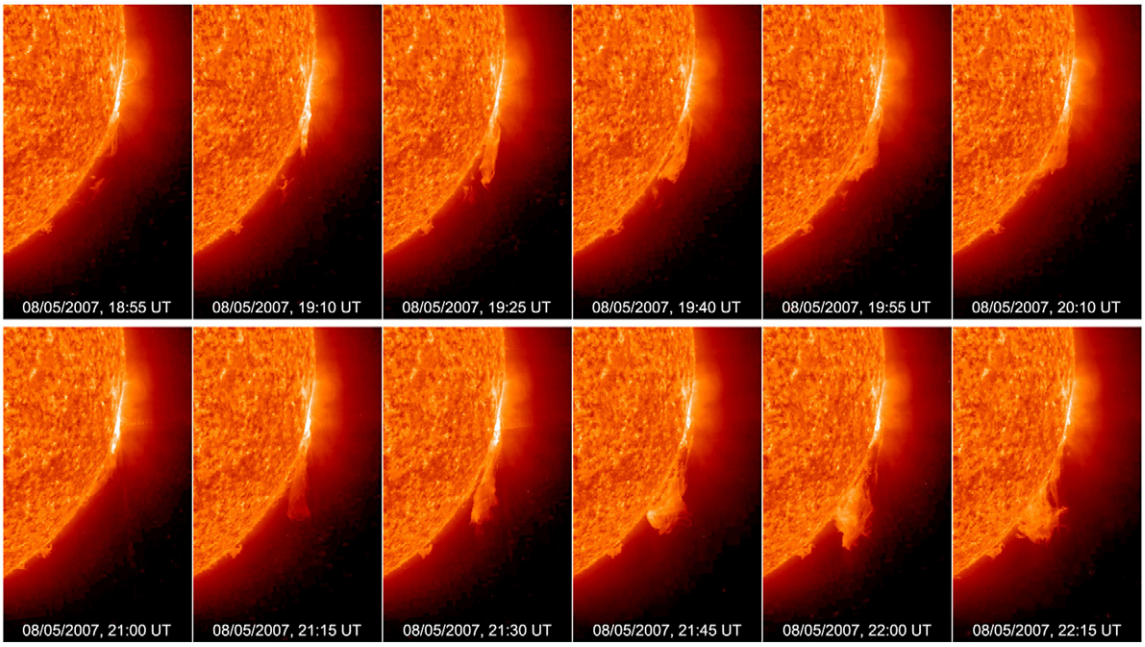

Figure 2. Two sequences of EUVI He II λ304 images acquired from *STEREO A* on the day before the eruption of 2007 May 9, when the AR 10953 was crossing the solar limb. These images show the occurrence of two successive "failed" eruptions from the AR boundary: in both cases, the "cool" chromospheric material, ejected southward, flows back toward the Sun propagating along the closed magnetic field lines.

(A color version of this figure is available in the online journal.)

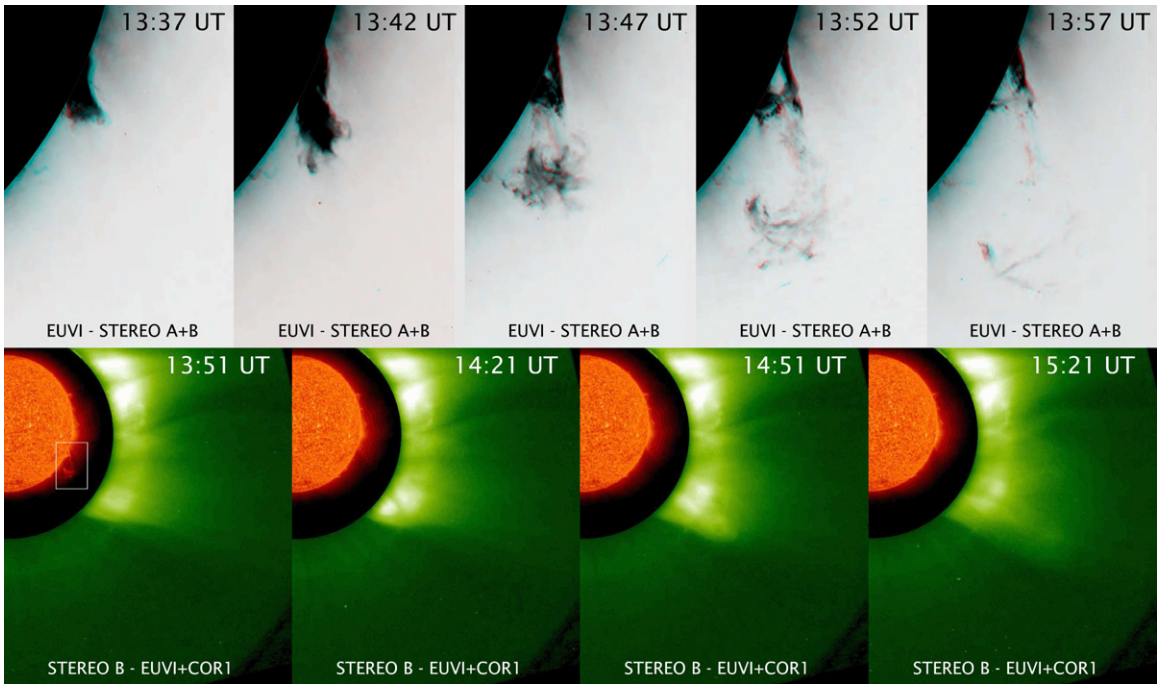

Figure 3. Top: a series of anaglyph EUVI He II λ304 images showing the eruption on 2007 May 9 (see the text for explanations). These images can be viewed in three dimension with standard anaglyph glasses having red and blue lenses for the left and right eyes, respectively. Bottom: a series of *STEREO B*/COR1 and *STEREO B*/EUVI He II images showing the evolution of the resulting CME (times are given in each image). The small rectangular box in the left image reproduces the size of the "zoomed" image shown in the top sequence at 13:52 UT.

acquired by the *SOHO*/MDI instrument show that such an instability possibly occurred because of the photospheric magnetic fields evolution (Figure 1, right column). MDI continuum images and MDI magnetograms show that AR 10953 includes a single negative polarity sunspot followed, in the sense of the solar rotation, by a disperse positive polarity region, hence the AR is mainly bipolar. Nevertheless, during the AR transit across the disk, a progressive emerging of new positive polarity regions occurs westward to the negative spot (Figure 1, panels b–d). This implies a transition from a bipolar to a multipolar magnetic configuration, hence an increase in the complexity of the overlying magnetic field topology. Subsequent changes in the overall closed field configuration above AR 10953 trapping the plasma continuously ejected and accumulated in the pre-

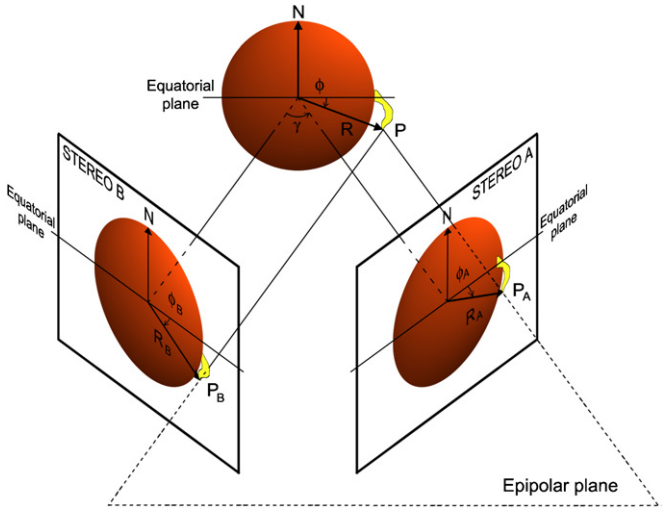

Figure 4. Cartoon showing the geometry of a contemporary observation from *STEREO A* and *B* of a prominence eruption. Given the two different projected altitudes (R_A and R_B) and latitudes (ϕ_A and ϕ_B) of the same point P, knowing the angular distance γ between the two spacecrafts, it is possible to derive via triangulation the 3D coordinates of this point.

(A color version of this figure is available in the online journal.)

vious days, may help the destabilization of the filament and the occurrence of the final eruption. The comparison between MDI magnetograms and Hα images also shows that the filament was aligned approximately with the separation line between the positive and negative polarities (i.e., along the neutral line), and that the northward and southward footpoints were located in the negative spot and in the disperse positive polarity region, respectively.

On 2007 May 9, when the AR 10953 is already behind the solar limb by $\sim$14° (longitude of $\sim$104° W measured from the central meridian), the large prominence eruption reported here occurred:[1] this event is shown in Figure 3 (top panels) as a sequence of *STEREO*/EUVI He II λ304 red and blue anaglyph images. Anaglyph images shown in Figure 3 have been created by rescaling each pair of frames acquired by *STEREO A* and *B* to a common center and image size.[2] In order to facilitate the 3D visualization a "zoom" centered on the prominence has been extracted and, after removing the disk emission, a further relative shift between the two images has been applied superposing the different views of the same structures. EUVI images in Figure 3 show a tongue of plasma that, anchored at an approximate latitude of $\sim$24° S, starts to expand southward around 13:40 UT. The prominence initially accelerates southward, then progressively rotates westward changing its direction of propagation. The eruption finally results in a slow ($v_{\rm CME} \sim 310$ km s^{-1}), decelerating ($a_{\rm CME} \sim -7.4$ m s^{-2}) limb CME[3] propagating around a latitude of 42° S (Figure 3, bottom panels). This CME has been observed by the two *STEREO A* and *B* EUVI telescopes; in the following section, I describe how EUVI He II λ304 pairs of images have been used to study the prominence 3D structure and expansion.

[1] Please notice that this event, occurred during a multi-spacecraft campaign, has been observed also by the *Hinode* EUV Imaging Spectrometer (EIS) and the *SOHO*/UV Coronograph Spectrometer (UVCS). Please refer to Bemporad et al. (2009) and Del Zanna et al. (2009) for preliminary results from these data.

[2] Please refer to Gissot et al. (2008) for a general description of the pre-registration *STEREO* geometry.

[3] See the LASCO CME catalog at http://cdaw.gsfc.nasa.gov/CME_list/.

3. EUVI DATA: THE TRIANGULATION TECHNIQUE

In order to derive the 3D shape and orientation of the erupting prominence, it is necessary to perform a triangulation study by comparing the pair images acquired from two different view points by the two *STEREO* spacecrafts. The geometry of the *STEREO* observations is sketched in Figure 4: if we assume for instance that a prominence is sitting above the limb (as seen from the Earth) at an altitude R and a latitude ϕ (top middle image), the same point P (the prominence edge in Figure 4) will be observed on the two *STEREO A* and *B* instruments in two different points P_A and P_B located at projected altitudes R_A and R_B and latitudes ϕ_A and ϕ_B, respectively (bottom right and left images in Figure 4). The three points P, P_A, and P_B define the so-called epipolar plane associated with the point P: such a plane is defined for any object point P. If the positions of points P_A and P_B with respect to the Sun center are known and these points correspond to the same 3D point P, given the angular distance γ between the two spacecrafts and by assuming that the epipolar planes can be considered all parallel to the ecliptic plane, it is possible to derive, by simple triangulation geometry, the 3D coordinates of each point P.[4]

Nevertheless, the main problem with this technique is to make the correct "pair association," i.e., to identify the position of the *same* feature in both images. In fact, the erupting plasma is optically thin, hence the emission at each pixel comes from an integration along two different LOSs, making things more complicated. For instance, a 2D plasma sheet could result relatively bright if observed edge-on and almost invisible if observed face-on. On the other hand, the 3D position of the center of a spherically symmetric plasma blob could be unambiguously identified, once the centroid of the EUV emission is selected in both the projected *STEREO* views. Hence, a way to reduce the uncertainties is to select only EUV features with a more spheroidal shape in both images (see Figure 5). In this case, the pair association has been possible, thanks to the presence across the prominence of many clearly identifiables spheroidal subfeatures (i.e., bright He II knots, blobs, subfilaments, or threads) present in both EUVI images; some of these features are outlined as an example in Figure 5 (left and right panels).

On 2007 May 9, the *STEREO A*–Sun–*STEREO B* angle γ was approximately $\gamma = 7\overset{\circ}{.}2$: this quite small angle guarantees that the projection effects mentioned above and related to the integration along two different LOSs are quite small. Nevertheless, thanks to the very high EUVI spatial resolution, this angle is sufficient to perform a triangulation study on the observed prominence.[5] In particular, on 2007 May 9, the Sun was observed by the two EUVI telescopes on *STEREO A* and *B* with a spatial resolution of 1.″45 pixel^{-1} and 1.″59 pixel^{-1}, respectively.[6] By taking an average resolution of $\sim$1.″5 pixel^{-1} for both instruments, a point source located for instance at an heliocentric distance of 1.2 $R_\odot$ above the limb projects in the two EUVI telescopes fields of view in two different points located at a relative projected distance $\sim$0.01 $R_\odot$ = 9.″6, hence $\sim$6.4

[4] Please refer to Mierla et al. (2008) for a better description of the *STEREO* triangulation geometry.

[5] Please note that the 3D filament study already performed by Gissot et al. (2008) refer to an event which occurred only $\sim$10 days after the eruption reported here, hence Gissot et al. (2008) had *STEREO* observational parameters very similar to the present case.

[6] I remind the reader that, even if the two EUVI telescopes are identical, the spatial resolution is not the same because the *STEREO A* spacecraft orbits closer to the Sun than *STEREO B*.

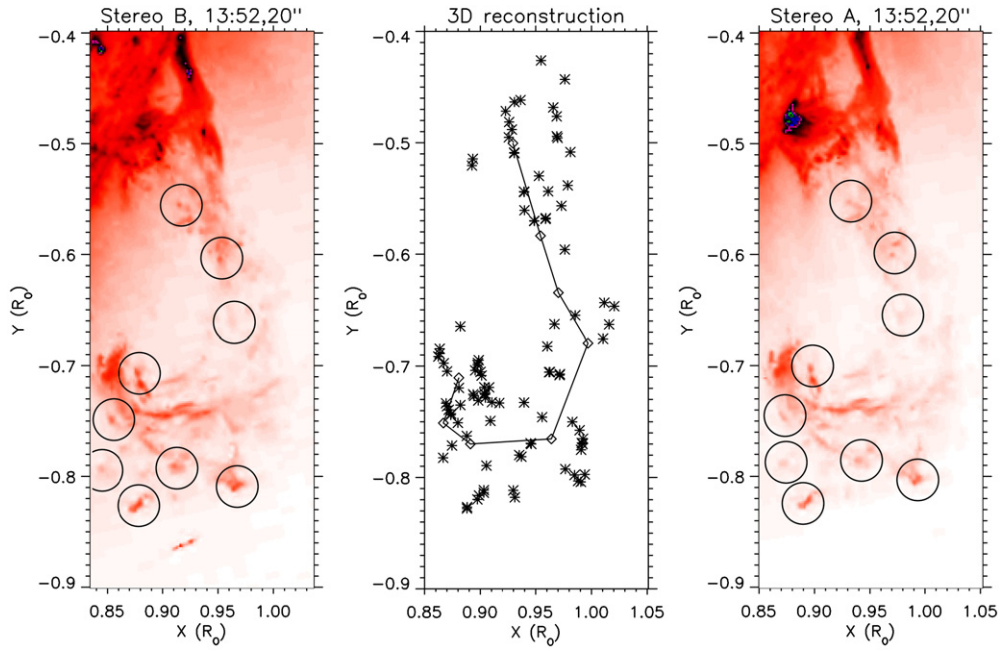

Figure 5. Pair of He II λ304 images acquired at 13:52 UT by *STEREO*/EUVI *B* (left panel) and *A* (right panel) and the 3D positions (reconstructed via triangulation) of the 100 pairs of features selected inside the prominence as seen from the Earth (middle panel). As an example, some of the selected pairs are outlined in the left and right panels by black solid circles. As a reference, the solid line in the middle panel shows an interpolation between the 100 points (see the text).
(A color version of this figure is available in the online journal.)

pixels on the two detectors. This implies that the displacement of the smaller EUV features due to the different location of the *STEREO A* and *B* spacecrafts can be resolved in each frames pair.

In this work, I selected 100 pairs of He II features in the two EUVI images acquired at 13:52, 20 UT (see also Figure 3). For the triangulation study, I used the routine available in the *STEREO* package of the SolarSoftware library (*scc_measure.pro*) which, after reading in a pair of *STEREO* EUVI *A* and *B* images, is able to trace the LOS of a point selected in one image pair into the field of view of the second image (the so-called epipolar line—see Thompson (2008b) for an example application of this routine to sungrazing comets). For each identified pair of spheroidal features, this routine has been used to infer via triangulation the 3D coordinates (i.e., altitude h, latitude θ, and longitude ψ) of the associated feature and to "reconstruct" the 3D shape of the erupting structure. For the present case, I empirically estimated that the uncertainties associated with the inferred coordinates are on the order of $\Delta\psi \simeq 4\%$, $\Delta\theta \simeq 1\%$, and $\Delta h \simeq 0.4\%$; results from this technique are described in the following section.

4. THE ERUPTING PROMINENCE THREE-DIMENSIONAL STRUCTURE AND EXPANSION

The reconstructed distribution of the 100 selected points inside the erupting prominence is shown in Figure 5 (middle panel) in the standard heliographic coordinate system, described in Figure 6 (panel a). In order to better show the 3D shape of the filament, the selected 100 points have been grouped into eight subclasses of closest points: the drawn solid line connects the eight interpolating points obtained by averaging the 3D coordinates in each subclass. It turns out that, at 13:52 UT, the prominence is mostly a "hook-shaped" structure with an approximate length (estimated as the sum of distances between the eight average points) $l = 0.43\ R_\odot$ and is centered at an average longitude of 14.°2 behind the limb (i.e., 104.°2 W from the central meridian), in very good agreement with the longitude of the source AR (see also, later on, Figure 8), and an average latitude of 34.°8 S (hence ∼24° southward with respect to the source AR). This implies that the early prominence plasma motion, finally resulting in a small CME propagating at a latitude of ∼42° S, has mainly no longitudinal component: the plasma expands only in altitude and in the latitudinal direction, hence over a plane. The 3D distribution of the eight interpolating points is also mainly planar: in the following, I demonstrate in particular that the 100 points have mainly a planar 2D distribution in the 3D space, i.e., that the erupting prominence material lies in first approximation over a plane.

If the prominence is planar, it is possible to define a new reference system $x'y'z'$ having the plane $x'O'y'$ coincident, in first approximation, with the prominence plane. The $x'y'z'$ system has been initially defined by placing the axes $x'y'z'$ parallel to the heliographic coordinate system axes xyz and the origin O' in correspondence of the median of the 100 points. If the prominence really lies over a plane, when observed with the LOS in a direction $\mathbf{v}_\perp$ perpendicular to its plane the intercepted thickness along this direction $d_{\mathbf{v}\perp}$ will be minimum. The average prominence thickness $d_{\mathbf{v}}$ on a 3D direction defined in general by a vector $\mathbf{v}$ is computed here as $d_{\mathbf{v}} = 2\sigma_{\mathbf{v}}$, where $\sigma_{\mathbf{v}}$ is the average standard deviation of the 100 points coordinates measured along an axis with direction $\mathbf{v}$ and origin O'. In order to find the direction $\mathbf{v}_\perp$, the three rotation angles around each one of the three coordinate axes (measured, as usual for right-handed reference systems, as positive if the rotation occurs in the clockwise direction around the axis as seen from the system origin) have been determined as follows. Because the prominence is mainly oriented parallel to the y-axis (see Figures 5 and 6, panel a), the system has been first rotated around the y'-axis by the angle $\alpha_{y'}$ able to minimize the thickness d_z along the z-axis (i.e., along the LOS); it turns out that $\alpha_{y'} = 54.°5$. Successively, the system has been rotated around the z'- and

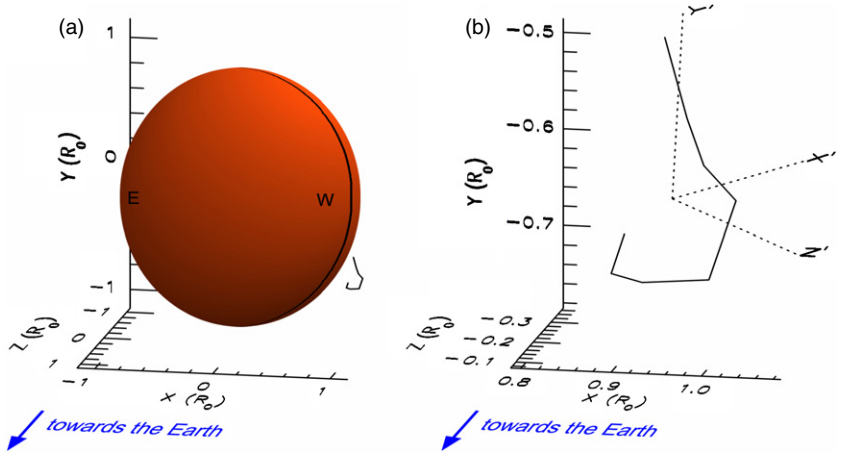

Figure 6. Panel a: the standard xyz heliographic coordinate system, having the origin O at the Sun center and the x-, y-, and z-axes pointing toward the west limb, the north limb, and the Earth, respectively. The solid curved black line on the Sun shows the position of the west limb as seen from the Earth. The relative position of the prominence inferred via triangulation is also shown in scale by using the same interpolating line of Figure 5. Panel b: a "zoom" on the prominence interpolating line, showing the relative position between the heliographic coordinate system (panel a) and the reference system $x'y'z'$ with origin O' on the median of the 100 selected points and the $x'O'z'$ plane coincident with the prominence plane (see the text).

(A color version of this figure is available in the online journal.)

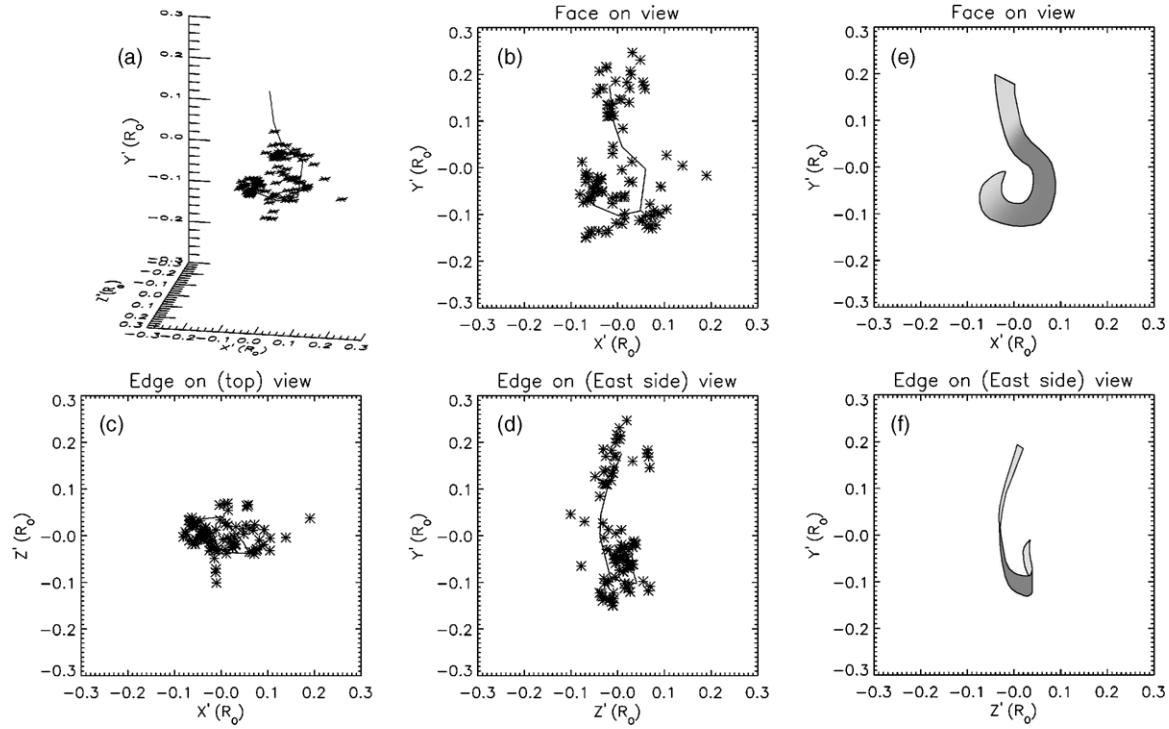

Figure 7. 3D distribution of the 100 selected points as seen in the $x'y'z'$ reference system (panel a) and the corresponding projections over the $x'O'y'$ (panel b—face-on view), $x'O'z'$ (panel c), and $z'O'y'$ (panel d—edge-on views) planes. The right cartoons show the prominence appearance (in the hypothesis of a "ribbon-shaped" feature) as seen if projected over the $x'O'y'$ (panel e) and $y'O'z'$ (panel f) planes (to be compared with the interpolating solid line in panels b and d).

x'-axes by the angles $\alpha_{z'} = 3.^{\circ}0$ and $\alpha_{x'} = 8.^{\circ}0$ able to minimize the thickness d_x and d_y computed along the x- and y-axes, respectively. Given the position of the origin O', the sequence of rotations by $\alpha_{y'}$, $\alpha_{z'}$, and $\alpha_{x'}$ angles finally defines the orientation of the new reference system $x'y'z'$ (shown in Figure 6, panel b) with respect to the heliographic system. In this system, the prominence thickness in the direction perpendicular to the $x'O'y'$ plane is $d_{\mathbf{v}\perp} \equiv d_{z'} = 0.061\ R_{\odot}$, while the extensions along the two directions x' and y' parallel to this plane are $d_{x'} = 0.11\ R_{\odot}$ and $d_{y'} = 0.23\ R_{\odot}$. Hence, the prominence length $l = 0.43\ R_{\odot}$ is $l \sim 7.0 \times d_{z'}$, indicating a mostly 2D planar structure. The 3D distribution of the 100 points as seen in the resulting $x'y'z'$ reference system is shown in Figure 7 (panel a), together with the projections over the three planes $x'O'y'$ (face-on view—panel b), $x'O'z'$ (panel c), and $z'O'y'$ (panel d). Figure 7 shows that the prominence points have a much larger spread in the $x'O'y'$ than in the $z'O'y'$ and $x'O'z'$ projections, as expected for a mainly planar feature lying over the $x'O'y'$ plane.

About 25–30 minutes after the beginning of the eruption (~13:40 UT) the prominence material is no more visible in the EUVI images. Nevertheless, thanks to the very high temporal resolution (~37 s) of these observations, it has been possible also to study the early 3D trajectories followed by

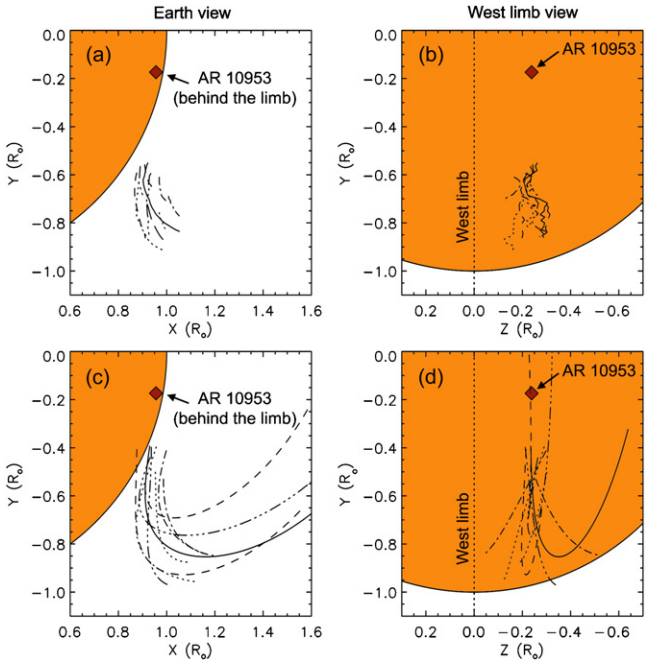

Figure 8. Reconstructed 3D trajectories of 10 He II λ304 features inside the erupting prominence as seen from an observer located at the Earth (panel a) and above the west limb (panel b); the corresponding extrapolated trajectories from the second-order polynomial fits are shown in the bottom panels. The dotted vertical lines in panels b and c represent the plane of the sky (hence the plane where trajectories are projected in panels a and b), the light gray shaded area corresponds to a visible portion of the solar disk and the dark gray diamond represents the center position of the AR 10953, located behind the west limb, as shown in panels b and c (see also panel a in Figure 6).

(A color version of this figure is available in the online journal.)

the erupting plasma. To this end, I selected 10 He II features that "survived" during the expansion over time intervals going from ∼5 up to ∼15 minutes. For each one of these features I performed again, frame-by-frame, the same triangulation analysis described above, deriving at each time h, θ, and ψ. The resulting 3D trajectories of these 10 features are shown in Figure 8 (in the standard heliographic reference system xyz) from two different points of view, together with the trajectories extrapolated from second-order polynomial fits. On the xOy plane (Figure 8, panels a and c), the plasma expands along "curved" paths (see also Figure 3, top panels): during the expansion the prominence material undergoes not only a radial acceleration a_r, but also a much stronger latitudinal acceleration a_θ ($a_r = 170.0$ m s^{-2} while $a_\theta = 5.98 \times 10^{-7}$ rad s^{-2}, which corresponds to $a_\theta = 500$ m s^{-2} at 1.2 $R_\odot$). Plasma trajectories on the yOz plane (Figure 8, panels b and d) are more uncertain, because of the larger error bars in the estimated longitudes ψ. Nevertheless, the estimated longitude changes are larger than the associated uncertainties (∼4%), hence it is possible, from a simple linear fit of the ψ versus t curves, to estimate in first approximation how the prominence expands along the LOS. It turns out that at 1.2 $R_\odot$ the average longitudinal speed of the prominence is small ($v_z \simeq 40$ km s^{-1} toward the observer), hence the prominence expands almost parallel to the plane of the sky.

The selected 10 He II "features" show a quite large spread in the derived velocities and accelerations. From these differences in the 3D trajectories, larger than the associated uncertainties, it is possible to estimate the 3D expansion factors of the prominence. First of all, by extrapolating all the h versus t curves back to the initial altitude $h_{\rm in} \simeq 1.08$ $R_\odot$ (see Figure 3), it turns out that the eruption start time is $t_{\rm in}$ =13:40 UT. At this time, the prominence extends in the radial, latitudinal and longitudinal directions respectively over $\Delta r_{\rm in} = 0.10$ $R_\odot$, $\Delta\theta_{\rm in} = 0.28$ $R_\odot$ and $\Delta\psi_{\rm in} = 0.17$ $R_\odot$, hence occupies an initial volume $V_{\rm in}$ on the order of $V_{\rm in} \sim \Delta r_{\rm in} \times \Delta\theta_{\rm in} \times \Delta\psi_{\rm in} = 1.6 \times 10^{15}$ km^3. At the beginning of the eruption at $t_{\rm in}$ =13:40 UT the prominence material is centered around a latitude $\theta = 24.^\circ3$ S and a longitude $\psi = 105.^\circ7$ W (i.e., 15.°7 behind the limb) while at the same time the source AR (centered at a latitude $\theta = 10.^\circ0$ S and a longitude $\psi = 104^\circ$ W, i.e., 14° behind the limb, see Figure 8) extends from the equator down to a latitude of $\simeq 20^\circ$ S. This implies that the prominence plasma erupts from the southward limb of the source AR, in good agreement with the observed position of the Hα prominence (Figure 1, panel e). Twenty minutes later, when the prominence material is at an average heliocentric distance of 1.4 $R_\odot$ and is almost invisible in the EUVI He II images (see Figure 3), the prominence extends in the radial, latitudinal, and longitudinal directions, respectively, over $\Delta r_{\rm fin} = 0.32$ $R_\odot$, $\Delta\theta_{\rm fin} = 0.61$ $R_\odot$, and $\Delta\psi_{\rm fin} = 0.19$ $R_\odot$, which implies a final volume $V_{\rm fin}$ on the order of $V_{\rm fin} \sim \Delta r_{\rm fin} \times \Delta\theta_{\rm fin} \times \Delta\psi_{\rm fin} = 1.3 \times 10^{16}$ km^3; hence, the total volume occupied by the prominence increases by a factor of ∼8 over the first 20 minutes.

5. DISCUSSION AND CONCLUSIONS

The 3D shape and trajectory of a prominence eruption occurred on 2007 May 9 (Figure 3) have been reconstructed here, thanks to the high spatial and temporal resolutions of the EUVI He II λ304 images acquired by the two *STEREO A* and *B* spacecrafts. Pair images acquired ∼12 minutes after the rising start time (∼13:40 UT) show that the prominence has mainly the shape of a "hook," with its base anchored at the Sun (Figures 5 and 6). Results from the triangulation study performed here lead to conclude that at this time the prominence length is ∼7 times larger than its thickness and that the erupting material is lying over a plane, mainly parallel to the north–south direction and inclined by 54.°5 with respect to the LOS direction (Figure 7). Interestingly, the radial, latitudinal, and longitudinal expansion factors estimated from the observed prominence 3D trajectory (Figure 8) are quite different, implying a non-isotropic expansion. The total volume occupied by the prominence increases in 20 minutes by a factor of ∼8, but the altitude radial and latitudinal prominence extensions increase by 220% and 120%, respectively, while the longitudinal extension increases only by 12%. Hence, at least in the early phase of the eruption reported here, during the expansion the prominence material tends to preserve its 2D planar distribution.

The high spatial resolution EUVI images (Figure 3) show inside the erupting prominence a very complex 3D spatial distribution of the erupting plasma, maybe with small-scale twisted structures rapping around each other. Nevertheless, the overall planar distribution of the prominence material in the early stage of the eruption and the successive "2D expansion" described above both suggest that globally the prominence does not have a twisted flux rope shape, as envisaged in all the flux rope–CME models, but is more similar to a ribbon-like structure. For a better visualization of this conclusion, such a ribbon-like structure has been tentatively drawn in the two cartoons shown in Figure 7 (panels e and f, to be compared with panels b and d, respectively). Filaments in ARs most clearly have in Hα the form of long thin ribbons and it has been argued that the occurrence of a ribbon-like filament eruption could be related to the presence or not of a small

bending around the axis dubbed "roll effect" (see, e.g., Martin 2003; Panasenco & Martin 2008). Results described above suggest that, despite the intrinsic complexity of the 3D plasma distribution on small scales, the erupting filament can be globally described as a 2D "ribbon," instead of a 3D twisted flux tube. The EUVI frames acquired in the minutes after the eruption start show that during the southward expansion the prominence turns westward, but it is hard to say from the estimated 3D trajectories if any "roll effect" is really present. The evident change in the direction of propagation could be due to an asymmetric configuration of the closed loops located above the prominence resulting in a net magnetic tension force pushing the plasma on one side (westward).

Recently, Thompson (2008a) inferred for a different event a prominence rotation by $\sim$140° during the eruption, in agreement with the idea of untwisting of a helical flux rope. In contrast, the 3D trajectories inferred for the prominence expansion object of this study do not show evidence for helical motions: the prominence, rooted $\sim$14° behind the limb, expands approximately parallel to the plane of the sky (Figure 8, panels b and d). However, this conclusion holds only for the evolution starting from $\sim$10 minutes after the beginning of the eruption (13:40 UT), because in the first EUVI frames (Figure 2, top left panels) it was impossible to identify the same He II features identified at later times. Hence, the occurrence of a prominence rotation and/or of a "roll effect" in the first $\sim$10 minutes of the eruption cannot be excluded.

The planar "hook-shaped" distribution of the prominence material found in the eruption reported here suggests also that in some CMEs the arch-shaped expanding feature often observed in white light coronagraphs and dubbed "CME front" could be really an almost 2D expanding arcade, instead of an optically thin hemispheric shell, in agreement for instance with results found by Ciaravella et al. (2003) from UVCS spectroscopic observations of another event. It is at present unclear if the CME fronts are really formed by the expansion of coronal loops overlying the expanding prominence or simply by plasma sitting in the overlying corona being compressed and pushed away by the prominence. Nevertheless, it is evident that in both cases (i.e., the "loop system" or "compressed plasma" interpretations) if the driver (i.e., the prominence) is expanding over a plane (as in our case), the fraction of involved corona intercepted by the prominence during its expansion will also lie mainly over a plane. As a consequence, only a small fraction of the overlying loop system will be pushed away (in the "loop system" interpretation), or alternatively only a small fraction of the overlying corona will be compressed and ejected (in the "compressed plasma" interpretation). This suggests that a 2D expanding prominence could possibly lead to the formation also of a 2D CME front, as the one reported by Ciaravella et al. (2003). Later on, at larger heliocentric distances the plasma radial and tangential accelerations are likely to change: in a future development of this work, I plan to perform a study on the 3D expansion of the associated CME by using the *STEREO* and LASCO observations acquired at larger altitudes and to compare results with those reported here below 1.4 $R_{\odot}$.

The author thanks O. Panasenco for useful discussions on the event initiation and on the prominence "roll effect" and the anonymous referee for useful comments which significantly improved the presentation of these results. The author acknowledges support from ASI/INAF I/035/05/0 contract. *STEREO* is a NASA mission.

REFERENCES

Antonucci, E., et al. 1997, Sol. Phys., 182, 293
Bemporad, A., et al. 2009, Proc. 2nd *Hinode* Science Meeting, in press
Brueckner, G. E., et al. 1995, Sol. Phys., 162, 357
Chen, J., et al. 1997, ApJ, 490, L191
Ciaravella, A., et al. 2000, ApJ, 529, 575
Ciaravella, A., et al. 2003, ApJ, 597, 1118
Cremades, H., & Bothmer, V. 2004, A&A, 422, 307
Curdt, W., Wilhelm, K., Feng, L., & Kamio, S. 2008, A&A, 481, L61
Del Zanna, G., et al. 2009, Proc. 2nd *Hinode* Science Meeting, in press
Dere, K. P., et al. 1999, ApJ, 516, 465
Feng, L., et al. 2007, ApJ, 671, L205
Gissot, S. F., Hochedez, J.-F., Chainais, P., & Antoine, J.-P. 2008, Sol. Phys., 252, 397
Inhester, B. 2006, Publ. Int. Space Sci. Inst., arXiv:astro-ph/0612649
Kaiser, M. L., et al. 2008, Space Sci. Rev., 136, 5
Kohl, J. L., et al. 1995, Sol. Phys., 162, 313
Martin, S. F. 2003, Adv. Space Res., 32, 1883
Mierla, M., et al. 2008, Sol. Phys., 252, 385
Michalek, G., Gopalswamy, N., & Yashiro, S. 2003, ApJ, 584, 472
Moran, T. G., & Davila, J. 2004, Science, 305, 66
Noci, G., Kohl, J. L., & Withbroe, G. L. 1987, ApJ, 315, 706
Panasenco, O., & Martin, S. F. 2008, in ASP Conf. Ser. 383, Subsurface and Atmospheric Influences on Solar Activity, ed. R. Howe, R. W. Komm, K. S. Balasubramaniam, & G. J. D. Petrie (San Francisco, CA: ASP), 243
Pizzo, V. J., & Biesecker, D. A. 2004, Geophys. Res. Lett., 31, L21802
Suleiman, R. M., Crooker, N. U., Raymond, J. C., & van, Ballegooijen A. 2005, in IAU Symp. 226, Coronal, Stellar Mass Ejections (Cambridge: Cambridge Univ. Press) 71
Thompson, W. T. 2008a, in American Geophysical Union, Fall Meeting 2008, 3D Reconstruction of an Erupting Prominence (Washington, DC: American Geophysical Union)
Thompson, W. T. 2008b, Icarus, 200, 351
Timothy, A. H., & Tappin, S. J. 2008, Sol. Phys., 252, 373
Wood, B. E., et al. 1999, ApJ, 512, 484
Wuelser, J.-P., et al. 2004, Proc. SPIE, 5171, 111
Xie, H., Ofman, L., & Lawrence, G. 2004, J. Geophys. Res., 109, A03109
Zhang, M., & Chye Low, B. 2005, ARA&A, 43, 103
Zhao, X. P., Plunkett, S. P., & Liu, W. 2002, J. Geophys. Res., 107, 1223